Journal of
Composites Science

MDPI

Article

Effects of Incorporating Small Amounts of Fe_3O_4 Nanoparticles into Epoxidized Natural Rubber: Chemical Interactions, Morphology and Thermal Characteristics

Omar S. Dahham [1,*] and Khalid Al-Zamili [2]

[1] Department of Chemical Engineering, Faculty of Engineering, University of Baghdad, Baghdad 10071, Iraq
[2] Department of Oil and Gas Refinery Engineering, University of Al-Farabi, Baghdad 10022, Iraq; dr.khalid@alfarabiuc.edu.iq
* Correspondence: omar.s@coeng.uobaghdad.edu.iq

Abstract

Nanocomposites were synthesized from epoxidized natural rubber (ENR-50) and magnetite (Fe_3O_4) at 1, 5, and 9 wt.%, respectively. Various analyses were conducted to gain comprehensive insight into the properties of the nanocomposites. It was found that the ring epoxide units can be opened and bonded with the Fe moieties of the magnetite to form an Fe-O-C structure, as shown in FTIR spectra at 690 and 700 cm^{-1}. Peaks in UV-vis spectra at the wavelength of 297 nm shifted to 299, 303, and 309 nm for the nanocomposite samples with 1, 5, and 9 wt.% Fe_3O_4, respectively. XRD showed a decrease in the amorphous peak intensity, while new diffraction peaks emerged at 33° and 43°, indicative of the crystalline structure of the Fe_3O_4 in the nanocomposites. Based on TEM micrographs, it was found that the average size of Fe_3O_4 particles in the rubber matrix with 1 wt.% Fe_3O_4 was around 20 and 33 nm. SEM micrographs proved that nanoparticles with 1 wt.% Fe_3O_4 were regularly dispersed in the rubber matrix, and that magnetite nanoparticles were spherical in shape, as well as having strong interactions and bonding with the rubber matrix. A TGA thermogram showed three thermal steps of degradation across a wide temperature range, from 81 °C to 592 °C, and resistance to thermal degradation of the nanocomposite samples as compared to the rubber sample could be clearly observed. Furthermore, DCS showed higher Tg for nanocomposites at 24.4, 25.1, and 26.3 °C, respectively, compared to purified ENR-50 at −18.6 °C.

Keywords: nanocomposites; magnetite; epoxidized natural rubber; filler/matrix interactions; morphology

Academic Editors: Flávio Camargo Cabrera and Carlos Henrique Scuracchio

Received: 24 June 2025
Revised: 4 August 2025
Accepted: 6 August 2025
Published: 12 August 2025

Citation: Dahham, O.S.; Al-Zamili, K. Effects of Incorporating Small Amounts of Fe_3O_4 Nanoparticles into Epoxidized Natural Rubber: Chemical Interactions, Morphology and Thermal Characteristics. *J. Compos. Sci.* **2025**, *9*, 434. https://doi.org/10.3390/jcs9080434

1. Introduction

In the last few decades, nanotechnology has become essential for the development of science and technology, because it relies on scale manipulation, with nanomaterials showing different and unique properties compared to macro–micro-scale materials; in turn, they have attracted much attention, mainly in the energy industry, environmental industry, food industry, and medical field, massively affecting the global economy [1]. The term nano refers to sizes ranging from 1 to 1000 nm. Nanoparticles have unique characteristics compared to sheer-sized particles, such as a high surface area-to-volume ratio, high activity, strong magnetic properties, and unique optical characteristics [1,2].

Among them, magnetic (Fe_3O_4) nanoparticles are extensively used in bio-analytical methods and biomedical applications. Magnetic fields usually encounter less background

interference when biotype samples are used, making the susceptibilities of biotype specimens almost trivial. Due to this benefit, biological specimens are very accessible to external magnetic fields [3,4]. Already, Fe_3O_4 nanoparticles have been integrated into the designs of a vast range of biomedical applications, like bio-imaging, analytical tools, contrast agents, bio-sensors, photoablation therapy, separation, signal markers, and other biomedical applications [5,6]. Iron oxide nanoparticles (IONPs) have been extensively utilized in several studies due to their chemical stability, biocompatibility, and high magnetic susceptibility. IONPs exhibit unique magnetic and electrical behavior due to their capability to transfer ions from Fe^{2+} to Fe^{3+}. In the field of biomedicine, IONPs that are smaller than 20 nm are usually employed, as they present superior magnetic characteristics. They are also more widely used in the biomedical field compared to other magnetic nanoparticles due to their superparamagnetic characteristics, their high magnetization saturation value, the nature of the surface, which means that they are more biocompatible than other nanoparticles, and their small particle size distribution (smaller than 100 nm) [5–7].

In the last few years, nanocomposites have become emerging materials used in numerous applications. Inorganic nanoparticles like metal oxides have been combined with organic materials like polymers, which, in turn, has led to the development of different multifunctional materials with characteristics adopted from the respective constituents [8]. Several studies have been conducted on polymer/IONP hybrids/composites. IONPs can be incorporated into suitable polymers to produce hybrids/composites with the required properties for utilization in several potential applications. Therefore, IONPs have been incorporated into biodegradable and biocompatible polymers like poly (D,L-lactide) (PDLLA) [9], L-lysine [10], poly (lactic-co-glycolic acid) (PLGA) [11], poly (N-vinyl pyrrolidone) (PVP) [12], and alginic acid [13]. These combinations of organic and inorganic materials can be smoothly utilized in numerous biomedical applications, like hyperthermia, cell separation, drug delivery, and magnetic resonance imaging (MRI). Other polymers, such as polyethylene oxide [14], polypyrrole [15], polyurethane [16], polyaniline [17], and natural rubber [18], have also been utilized in research to formulate polymer/Fe_3O_4 hybrids. These hybrids possess different potential utilizations in magnetic materials, electromagnetic wave absorbers, capacitors, batteries, and solar and/or fuel cells.

Epoxidized natural rubber (ENR) is an improved natural rubber (NR) that is formed from natural rubber through a process called epoxidation, using formic/acetic peroxide in a certain reactor [19]. ENR comprises two types of functional groups: alkenes (C) and epoxides (E). These groups are distributed randomly throughout the backbone of rubber. In ENR, the reactive sites of alkene groups (C) are the double bonds that are involved in the crosslinking reaction, while the reactive sites of epoxide groups (E) are the rings that are involved in the ring-opening reaction (ROR). The ROR of ENR usually refers to the chemical reaction whereby the epoxide unit (oxirane) is opened by a nucleophile; this type of reaction is extensively used to modify and improve the reactivity and compatibility of composites, and this has been demonstrated in some of our previous work with the use of certain chemicals/solutions [20,21].

Therefore, ENR shows two different reactive sites that can be incorporated with any inorganic moieties at the nanoscale [21]. ENR exhibits high flexibility and polarity, a low glass transition temperature (T_g), good adhesion, and elastomeric characteristics, which has led to the wide utilization of this rubber in different applications such as lithium cells [21] and gas membranes [22]. Several studies on the nanocomposites of polymers and inorganic substances have used ENR as the host organic polymer. Mahmood et al. successfully formed a composite film from ZrO_2 and ENR using the sol–gel technique [23]. Their findings suggested that the chemical bonding between ZrO_2 and ENR increased as the proportion of ZrO_2 increased. In addition, the composite presented enhancements in

the optical transparency and thermal behavior as compared to ENR alone. The improved transparency shown in ENR/ZrO_2 nanocomposites may result from the reduction in or removal of light-scattering particles inherent in the manufacturing process. Other work has successfully synthesized and characterized different nanocomposites formed from ENR and SiO_2 [24], GNP [25], and CCTO [26].

On the other hand, Barrera et al. have synthesized epoxy/magnetite and studied the structural aspects of the nanocomposites [27]. They found strong interactions between filler (magnetite) and matrix (epoxy) that in turn led to improvements in the cross-linking density due to the contribution of magnetite. These improvements support the suggestion that the magnetite nanoparticles are able to perform not only as a rigid filler in the matrix, but also as a densifier of cross-linking, and this led to increases in the cross-link density.

Our previous work studied the influences of titania on the structural aspects, optical characteristics, thermal behavior and morphology of nanocomposite materials formed from ENR-50 matrix and TiO_2 nanoparticles. It is found that the presence of titania precursors in ENR-50 formed strong interactions via covalent bond (Ti-O-C), which affected some properties of the ENR-50/TiO_2 nanocomposites [28]. Another work was conducted to characterize the influences of different precursors (zirconia) on ENR-50; results suggested clear improvements on the thermal characteristics of the ENR-50/ZrO_2 nanocomposites [29–31]. However, there are only limited studies conducted on the incorporation of ENR with Fe_3O_4. The study conducted by Tan and Bakar was dedicated to the electrical conductivity of the nanocomposites synthesized from magnetite and ENR; their results showed that the electrical conductivity of the nanocomposites was enhanced as the content of magnetite increased [32]

Therefore, the current work aimed to present a comprehensive characterization for the ENR-50/ Fe_3O_4 nanocomposites and investigated the effects of different Fe_3O_4 content on the morphological changes, structural aspects, optical characteristics and thermal behavior of the synthesized nanocomposites.

2. Experimental

2.1. Materials

The ENR at 50 percent epoxidation was obtained from the Institute of Rubber Research in Kuala Lumpur, Malaysia; the specifications of ENR-50 are listed in Table 1. It was then prepared according to the purification process [21]. Iron (II) sulfate heptahydrate 99.5% ($FeSO_4 \cdot 7H_2O$) and potassium hydroxide (KOH) were purchased from Merck & Co., Inc., Rahway, NJ, USA. Toluene and tetrahydrofuran (THF) solvents were obtained from (Fisher Chemicals, Leicestershire, UK), while ethyl alcohol 99.9% dehydrated was provided by KSFE Sdn. Bhd., Petaling Jaya, Malaysia. All the above chemicals were utilized without any additional process unless otherwise mentioned.

Table 1. Chemical and physical specifications of ENR-50.

Characteristic	Value/Unit
M.Wt.	600,000 g/mol
MV	75
T_g	−21 °C
ρ	0.94 g/cm^3
Epoxide	50 mol%

2.2. Purification of ENR-50

The purification of rubber was achieved when 20 g of ENR-50 was dissolved in 400 mL of solvent (chloroform) and stirred at 25 °C temperature for 24 h, then the prepared mixture was filtered using cotton gauze to remove the impurities in ENR-50. Also, the precipitation process was conducted to the ENR-50 mixture by adding n-hexane, then the precipitate ENR-50 was transferred to a Petri dish and kept for 48 h at room temperature. Additional drying was carried out on the precipitate ENR-50 via vacuum oven at 60 °C for 2 days. The samples after the 2nd stage of drying represent the purified ENR-50.

2.3. Synthesis of ENR-50/Fe_3O_4 Nanocomposite Materials

The formation of Fe_3O_4 nanoparticles was conducted based on Bakar et al. [33], while the formation of ENR-50/Fe_3O_4 nanocomposites was conducted when three different samples were prepared using 1, 5 and 9 mg of $FeSO_4$ $7H_2O$; these were separately dissolved in 5 mL of distilled water. Then, 100 mg of purified ENR-50 was dissolved in 10 mL of Toluene. Ethanol (2 mL) was also added to the last mixture and left for stirring for 2 h; the stirring process was applied to dissolve all the purified ENR-50 in the solvent. After stirring was complete, the prepared mixture was heated at 75 °C temperature. During stirring and heating processes, 1 mL of potassium hydroxide (KOH, 2.5 M) was gradually added into the mixture with the same stirring and temperature conditions for another 2 h. Upon completion, all three samples were cooled to room temperature and placed in a Petri dish for 24 h to achieve the full evaporation of solvent in the mixture. The samples were then well washed several times with deionized water and ethanol to remove any soluble byproducts and unreacted KOH. Further drying was conducted on the samples using a vacuum oven at 50 °C temperature for 24 h.

2.4. Characterization of ENR-50/Fe_3O_4 Nanocomposite Materials

2.4.1. Fourier Transform Infrared Spectroscopy (FTIR)

An FTIR device from Perkin Elmer company, Shelton, WA, USA (model 2000) was utilized to characterize the nanocomposite samples. A film of each sample was placed on a window of zinc selenide at 25 °C temperature and then scanned (4000–600 cm^{-1}) of 0.4 cm^{-1} resolution. An average of 16 scans were applied on the sample.

2.4.2. X-Ray Diffraction (X-RD)

The purity/crystallinity of rubber and nanocomposites were examined via X-Ray diffraction from Philips, Amsterdam, Netherlands (X'Pert PW 3040 Powder); the device is attached with a mono-chromatic radiation filter (Cu-Ka) at 0.154 nm wavelength. All prepared samples were examined from 5 to 70° with 4°/min scan rate.

2.4.3. Thermal Gravimetric Analysis (TGA)

The TGA was conducted using a TGA analyzer with model of Perkin Elmer-4000, Shelton, WA, USA. All prepared samples were applied to the heating process with the range of 30 to 900 °C temperature, while the heating rate was set at 20 °C/min. The nitrogen gas was used in the analyzer during the heating process of all samples.

2.4.4. Differential Scanning Calorimetry (DSC)

The DSC was performed via DSC analyzer with a model of Perkin Elmer Pyris-6 (Shelton CT), Shelton, WA, USA. An aluminum pan was used to seal all prepared samples and then the heating process was applied in the range of −40 to 140 °C, while the heating rate was 20 °C/min. The nitrogen gas was used in the analyzer during the heating process of all samples. The heating process was then reversed from 140 to −40 °C and heating was applied again to reach to 140 °C with the same heating rate. The use of two heating cycles

is to remove any thermal history of the samples; the second heating cycle was applied to provide more accurate values of Tg. Therefore, the DSC results were obtained from the last heating process.

2.4.5. Scanning Electron Microscopy (SEM)

SEM analysis was conducted via SEM device (model: JEOL/JFC/6460/LA), Tokyo, Japan and run at 10 kV. During preparation, the samples were coated with a gold layer (1.5–2.5 nm thickness) to avoid any electrostatic charge that may occur; this coating could also improve the resolution of the images/micrographs during examination.

2.4.6. Transmission Electron Microscopy (TEM)

SEM examination of TEM was also used in this study to prove the nanoscale and structure of metal oxide in the rubber matrix. The micrographs of TEM were recorded by TEM analyzer, Tokyo, Japan (model: Jeol/JEM-1230), which was run at 20 kV. The samples were partially dissolved in tetrahydrofuran solvent (analytical grade) and the prepared suspension was dropped (2–3 drops) onto a copper grid with 200 mesh size and air-dried prior to examination.

2.4.7. Ultraviolet–Visible (UV–Vis) Microscopy

The UV–Vis microscopy from Perkin Elmer company, Shelton, WA, USA with model of Lambda 35 was utilized to examine the optical characteristics of the prepared samples. All samples were dissolved in tetrahydrofuran solvent (analytical grade). The examination was conducted with a wavelength range from 200 nm to 545 nm at 1 nm resolution.

3. Results and Discussion

3.1. Structure

Figure 1 shows the FTIR spectra of prepared samples (ENR-50 and ENR-50/Fe_3O_4 nanocomposites at 1, 5 and 9 wt.% of Fe_3O_4, respectively). According to the results, the range of characteristic band between 880 and 885 cm^{-1} belonged to the stretching vibration of epoxy groups of ENR-50 [21,22], whereas the characteristic band at 1070 cm^{-1} referred to the asymmetric/symmetric stretching of carbon-oxygen (C-O) functional group. Furthermore, the small stretching band found between 1240 and 1245 cm^{-1} usually belonged to the entire ring of epoxy structure (C-O-C). The two sharp bands in the ranges of 1388–1390 cm^{-1} and 1458–1460 cm^{-1} corresponded to the backbone distortion of hydrocarbon for CH_2 and CH functional groups. The small band shown at 2849–2851 cm^{-1} referred to the symmetry stretching of CH_2, while the bigger bands at 2911–2913 cm^{-1} and 2970–2973 cm^{-1} indicated the symmetry and asymmetry stretching of CH_2 and CH_3, respectively; this is consistent with what has been studied in previous works on ENR-50 structure [28].

For ENR-50/Fe_3O_4 nanocomposites, it is clearly observed that the presence of metal oxide (Fe_3O_4) has shifted the intensity of hydroxyl functional group in the range between 3415 and 3420 cm^{-1}; this is also consistent with the slight shift occurring in the stretching band between 878 cm^{-1} and 882 cm^{-1} of epoxy groups. This shift probably indicates the opening reactions of epoxide ring in the rubber, which suggested possible interactions between OH group of Fe_3O_4 surface and oxirane of the rubber. The shifting of wavelength between 878 cm^{-1} and 882 cm^{-1} referred to the C-O asymmetric stretching of the oxirane (epoxy ring). When Fe_3O_4 interacted with ENG-50, the stretching band shifted to a new wavelength representing a ring opening reaction of epoxy units in the presence of Fe^{3+} ions from Fe_3O_4 and/or hydroxyl groups (OH). Furthermore, the range of wavelength between 1650 cm^{-1} and 1652 cm^{-1} probably belonged to the double bond of Carbone = Carbone

(C = C) functional group. The presence of new peaks in the nanocomposites at the wavelength range between 690 cm^{-1} and 700 cm^{-1} is related to the vibrations of metal oxide and oxygen (M-O), which probably referred to the Fe-O vibration. Takai et al. have prepared nanoparticles of magnetite using sol-gel technique; the results showed that new characteristic peaks formed at the wavelengths of 688 cm^{-1} and 743 cm^{-1}, which referred to the formation of Fe-O vibrations [31]. Therefore, the characteristic peaks at 690 cm^{-1} and 700 cm^{-1} in the current study may also refer to successful interactions of the metal oxide with the rubber.

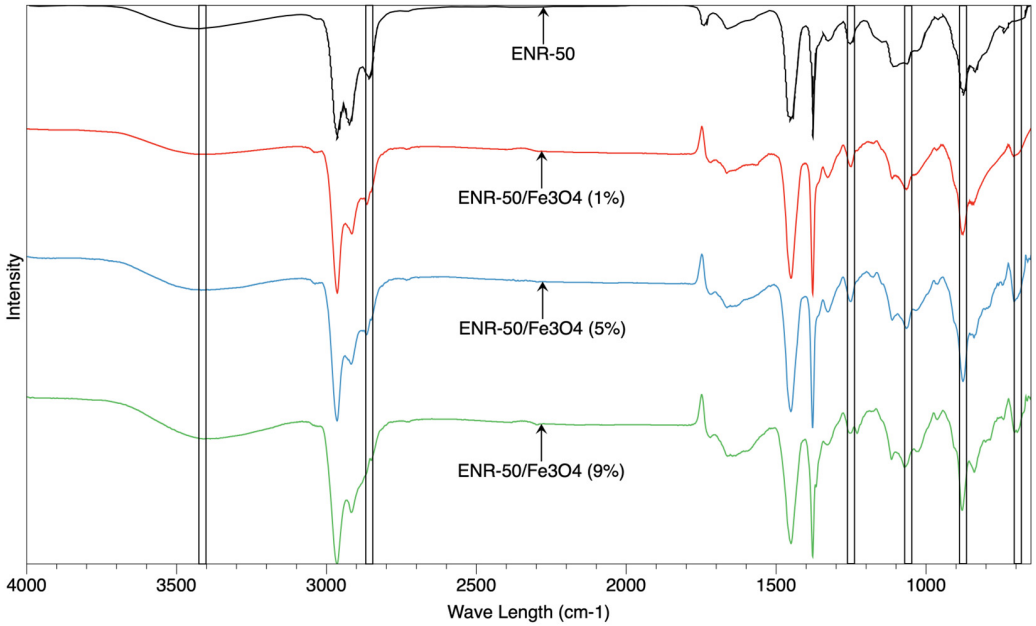

Figure 1. The spectra of FTIR of purified ENR-50 sample and ENR-50/Fe_3O_4 samples with different Fe_3O_4 content.

Figure 2a shows the X-ray diffractogram of Fe_3O_4 sample as a control, while Figure 2b shows the X-ray diffractogram of the prepared samples (ENR-50 and ENR-50/Fe_3O_4 nanocomposites at 1, 5 and 9 wt.% of Fe_3O_4, respectively). The prepared nanocomposites revealed new diffraction peaks at 33° and 43°, suggesting that the nanoparticles are preserved in the form of crystalline during the incorporation with the ENR-50.

The intensity increased as the content of magnetite increased in the nanocomposites, which is consistent with the previous work conducted by Motaung et al. [33], and the peak of amorphous form for the rubber presented in all diffractograms at about 20–21°. Nevertheless, the visible decrease in the intensity in the amorphous form, which is associated with new peaks, appeared for the crystallization form at 33° and 43°. These changes in the diffraction peaks presented a new form for the rubber matrix, which is a clear indication of the presence of the nanoparticles in the ENR-50 [34].

Figure 3 shows the UV spectra of the prepared samples (ENR-50 and ENR-50/Fe_3O_4 nanocomposites at 1, 5 and 9 wt.% of Fe_3O_4, respectively). Two characteristic peaks are clearly detected in the ranges of 251–257 nm and 297–309 nm in the rubber sample. The first peak located at 251–257 nm wavelength is related to the C = C transition ($n - \pi^*$), whereas the second peak located at 297–309 nm wavelength is related to the non-bonding electron transition of the epoxide [23]. These two characteristic peaks of the rubber also emerged in all nanocomposite samples. The first peak of all samples appeared between 251 and 257 nm wavelength, while the second peak clearly appeared between 297 and 309 nm wavelength. For nanocomposite samples, Table 2 shows that the second peak at 297 nm moved to 299, 303 and 309 nm for the nanocomposite samples at 1, 5, and 9 wt.%

Fe_3O_4, respectively; this shifting indicated that there are interactions between rubber matrix and magnetite [28]. Consequently, these findings have presented further observations on the rubber–magnetite interactions; the increase in magnetite content in the rubber matrix maximized the interactions. The type of rubber/metal oxide interaction was due to the oxirane reactions of epoxides in rubber that in turn created covalent bonds with the Fe moieties of Fe_3O_4 (Fe-O). This argument was also supported by the discussion of FTIR spectra of ENR-50/Fe_3O_4 samples.

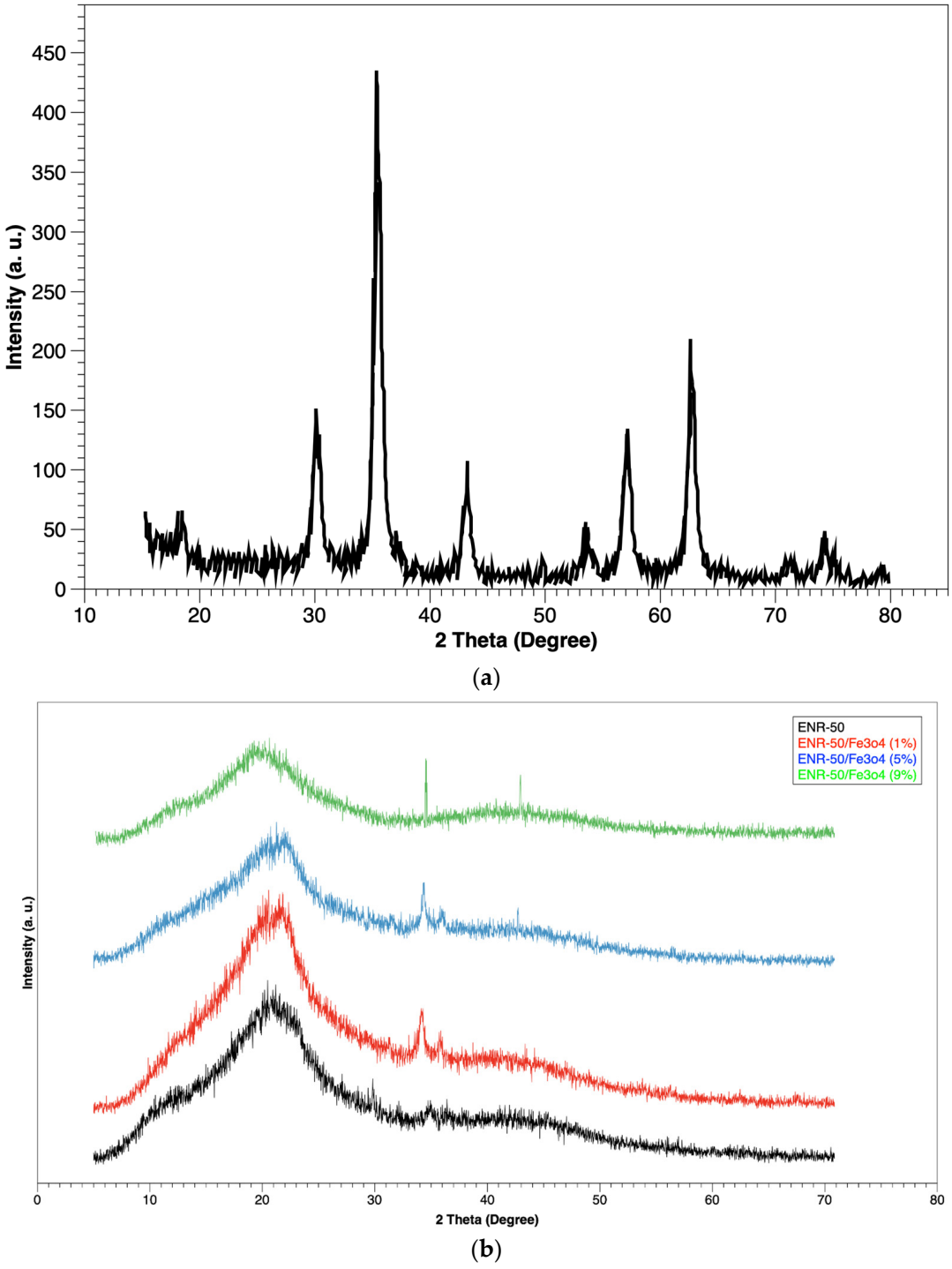

Figure 2. XRD of (**a**) Fe_3O_4 sample and (**b**) purified ENR-50 sample and ENR-50/Fe_3O_4 samples with different Fe_3O_4 content.

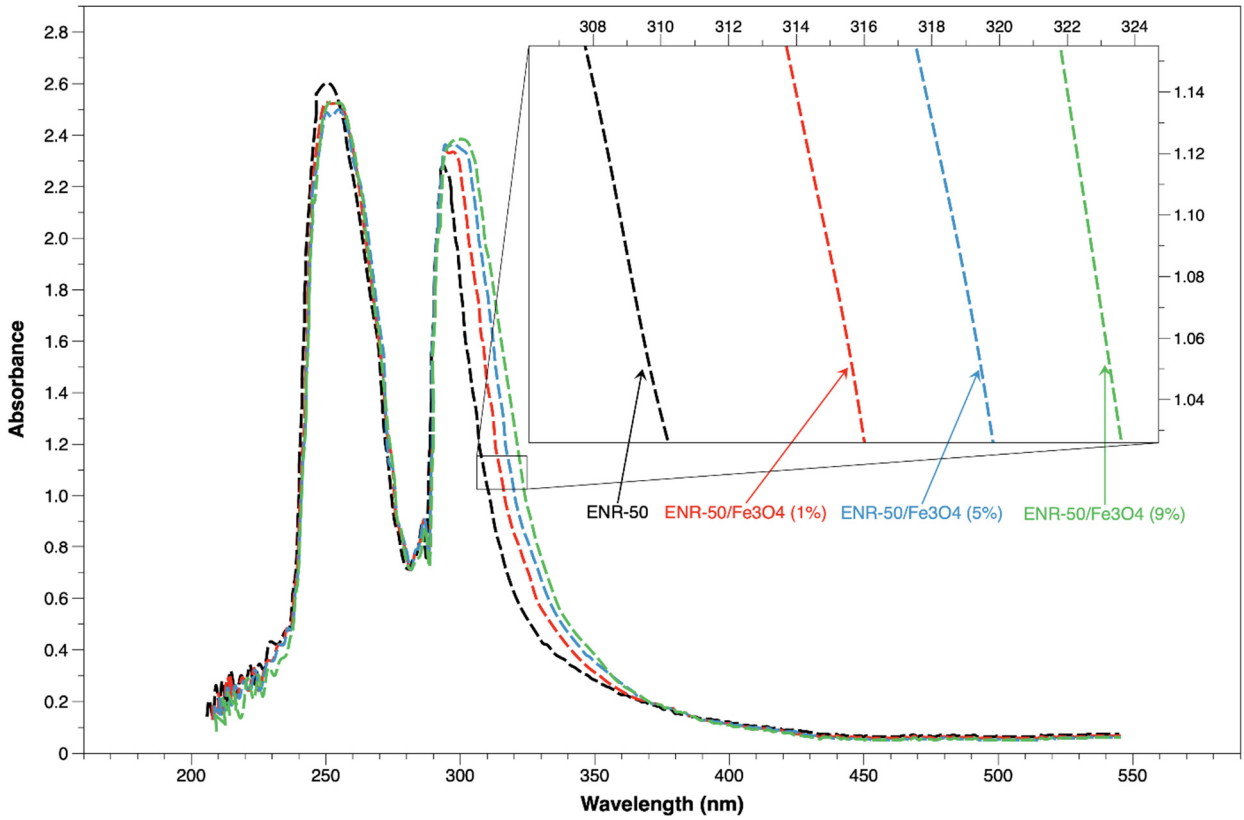

Figure 3. UV-Vis of purified ENR-50 sample and ENR-50/Fe_3O_4 samples with different Fe_3O_4 content.

Table 2. The shifting of UV-vis peaks due to ($n - \pi^*$) transition of non-bonding electrons for epoxide in the nanocomposites with different magnetite content.

Specimens	($n - \pi^*$) Transition (nm)
Purified ENR-50	297
ENR-50/Fe_3O_4 (1 wt.% of Fe_3O_4)	299
ENR-50/Fe_3O_4 (5 wt.% of Fe_3O_4)	303
ENR-50/Fe_3O_4 (9 wt.% of Fe_3O_4)	309

3.2. Morphology

The morphological characteristics of the ENR-50 and ENR-50/Fe_3O_4 nanocomposites at 1, 5 and 9 wt.% of Fe_3O_4 were investigated via FE-SEM and TEM analyses, respectively. The micrographs of the rubber/magnetite nanocomposites at 1, 5, and 9 wt.% of Fe_3O_4 are shown in Figure 4a, Figure 4b and Figure 4c, respectively. It is found that the Fe_3O_4 at 1 wt.% was regularly dispersed in the rubber matrix (Figure 4a) and the magnetite nanoparticles were in spherical shapes as well as having strong interactions with the rubber matrix. Furthermore, the morphological characteristics of the rubber matrix were altered through the synthesis of the ENR-50/Fe_3O_4 nanocomposites. The dispersion of magnetite nanoparticles at 5 wt.% persisted well enough in the rubber matrix (Figure 5b). While the highest magnetite content (9 wt.%) revealed clear agglomerations of nanoparticles in the rubber matrix (Figure 4c), these agglomerations have distorted the spherical structure of the Fe_3O_4 nanoparticles.

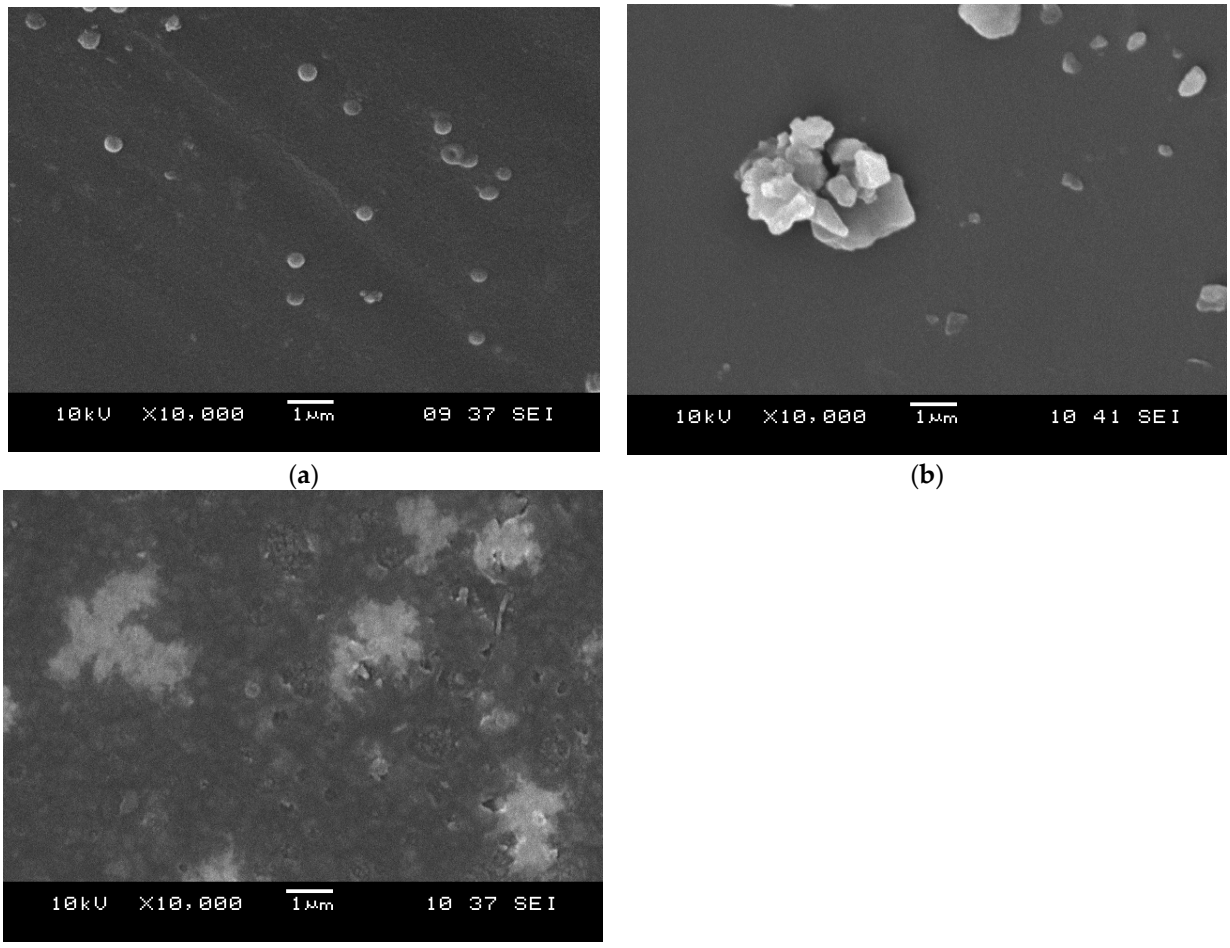

Figure 4. SEM micrographs of ENR-50/Fe_3O_4 samples at (**a**) 1 wt.%, (**b**) 5 wt.% and (**c**) 9 wt.% of Fe_3O_4 content.

The TEM analysis was utilized as a sufficient technique to estimate the particle size of the magnetite and also the dispersion of the metal oxide inside the rubber matrix. The micrographs of the rubber/magnetite nanocomposites at 1, 5, and 9 wt % of Fe_3O_4 are exhibited in Figure 5a, Figure 5b and Figure 5c, respectively. It is found that the average size of Fe_3O_4 particles in the rubber matrix at 1 wt.% Fe_3O_4 was around 20 and 33 nm, whereas the size of particles at 5 wt.% Fe_3O_4 was around 40–88 nm. Though the highest metal oxide content at 9 wt.% Fe_3O_4 exhibited different characteristics compared to lower Fe_3O_4 contents in the rubber matrix, the size of magnetite was immeasurable and the particles lost their spherical shapes; this was due to the clear aggregations of the nanoparticles formed in the rubber matrix, as shown in Figure 4c. The findings of TEM are consistent with the SEM micrographs. Ting has successfully synthesized different nanocomposite samples from the metal oxide (magnetite) mixed with thermoplastic (PE) and thermoset (epoxy resin). According to the morphological analyses (SEM and TEM), it is found that the magnetite has approximately a spherical form. The researcher has also found that the aggregations of magnetite could be due to the high level of interactions of magneto-dipole between the magnetite particles [35]. There was a clear discrepancy of nanoparticle sizes that were examined by FE-SEM and TEM. Usually, the FE-SEM micrographs presented larger particle sizes due to the agglomeration of nanoparticles (Fe_3O_4) in the rubber matrix, whereas the TEM micrographs show visualizations with higher resolution of Fe_3O_4 nanoparticles, which resulted smaller size measurements. These differences are anticipated, as FE-SEM

analysis focuses on surface changing, while TEM analysis presents an excellent observation of the particles at the nanoscale.

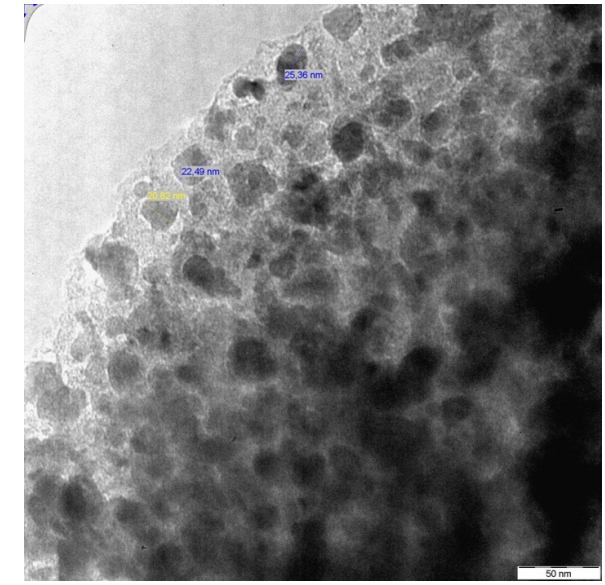

(**a**)

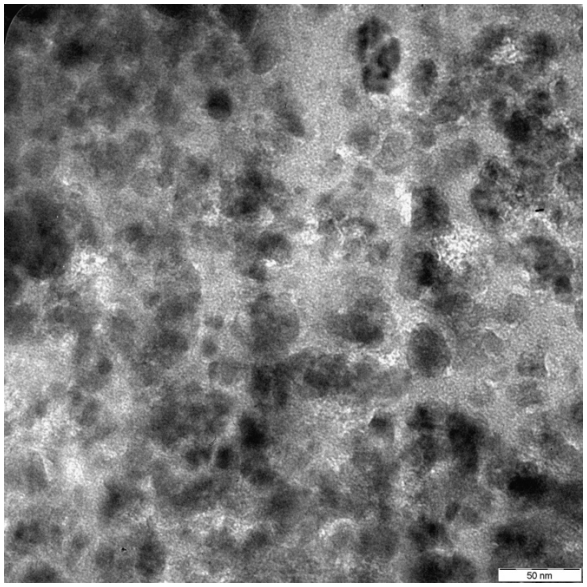

(**b**)

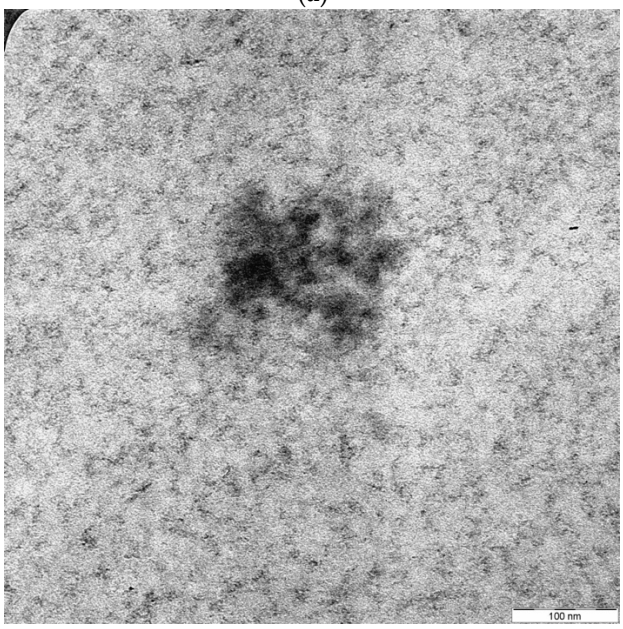

(**c**)

Figure 5. TEM micrographs of ENR-50/Fe_3O_4 samples at (**a**) 1 wt.%, (**b**) 5 wt.% and (**c**) 9 wt.% of Fe_3O_4 content.

3.3. Thermal Characteristics

The thermal behavior of the purified ENR-50 and prepared ENR-50/Fe_3O_4 nanocomposites at 1, 5 and 9 wt.% of Fe_3O_4, respectively, were investigated via thermal gravimetric analysis (TGA) and differential scanning calorimetry (DSC) analyses, respectively. According to the TGA curves shown in Figure 6, the rubber sample has exhibited two thermal steps of degradation; the first degradation (minor) was in the range of 81–105 °C, and this step occurred due to the evaporation of solvent and/or moisture that is trapped in the rubber matrix throughout the process of rubber preparation, whereas the second degradation (major) was in the range of 359–468 °C, and this step occurred due to the huge thermal degradation of rubber matrix (ENR-50) [36]. For prepared ENR-50/Fe_3O_4 nanocomposites,

all samples presented three thermal steps of degradation in a wide range of temperatures, from 81 °C to 592 °C. The first step of degradation was recorded between 83 °C and 129 °C, which refers to the evaporation of solvent, moisture and stuck residues in the prepared samples [37]. The second thermal step of degradation was the major weight percentage loss of the nanocomposites, which was between 288 °C and 525 °C. This led to a degradation of about 70 wt.% of the rubber matrix. Also, it is found that the second thermal degradation of all nanocomposite samples was shifted to a higher temperature as compared to the purified rubber sample. Through the pyrolysis process, the decreases occurring in the temperature of degradation of the nanocomposites could be due to the residual ions (Fe^{2+}) obtained from magnetite nanoparticles, which are known to increase the reactions of chain session, initiating thermal degradation at lower temperatures. The residual of potassium hydroxide (KOH) has also accelerated the chain opening reaction. Conversely, the nanocomposites showed increases in the temperature for the main thermal degradation compared to ENR-50 due to the strong interactions between nanoparticles and rubber matrix. These matrix/filler interactions have generally improved the thermal stability of the rubber/filler system via restricting the mobility of polymer chains [37]. The presence of nanoparticles in rubber matrix acted as a physical barrier, which in turn hindered the diffusion of volatiles from the bulk of prepared samples.

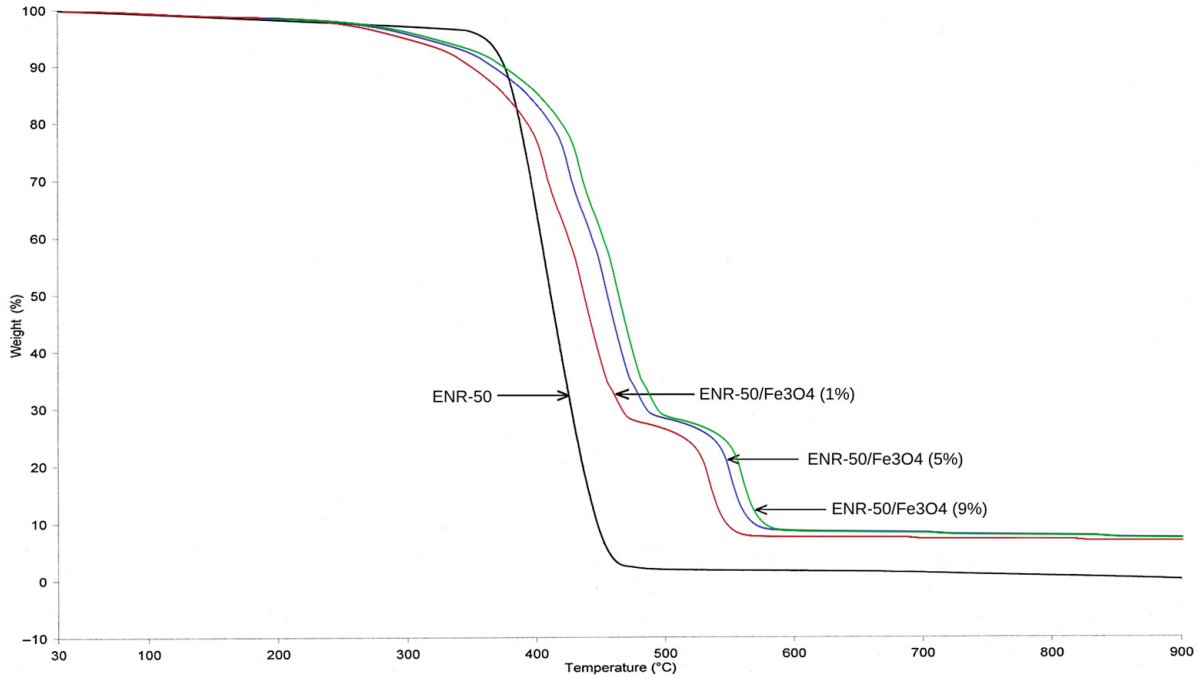

Figure 6. TGA thermogram of purified ENR-50 sample and ENR-50/Fe_3O_4 samples with different Fe_3O_4 content.

For obtaining further thermal assessment, DSC analysis was conducted on all samples, as shown in Figure 7. The samples of ENR-50/Fe_3O_4 nanocomposites at 1, 5 and 9 wt.% presented higher single glass transition (T_g) at 24.4 °C, 25.1 °C and 26.3 °C, respectively, than purified ENR-50 sample at −18.6 °C. The single T_g of samples was considered a sign of strong interactions between the rubber matrix and the metal oxide nanoparticles [38]; the increased T_g value of the nanocomposites could also be due to the ring opening reaction that produces vicinal glycolic OH groups, which in turn led to significant increases in intermolecular attractions (H bonds).

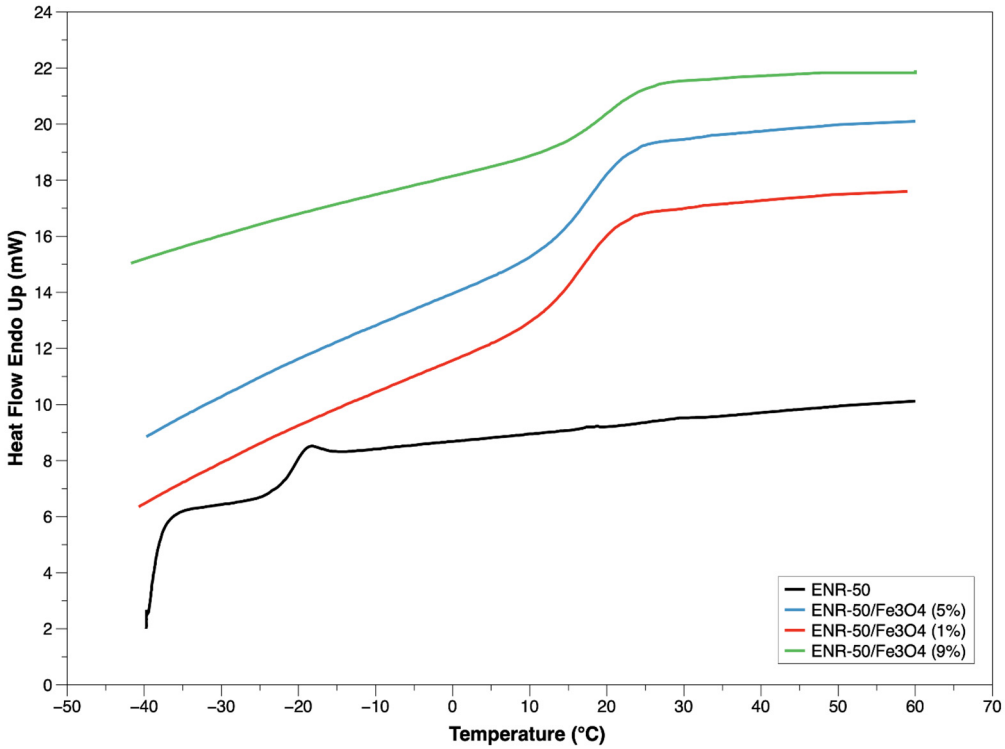

Figure 7. DSC thermogram of purified ENR-50 sample and ENR-50/Fe_3O_4 samples with different Fe_3O_4 content.

According to our previous work, it is found that the epoxide ROR% in the rubber had a straight impact on the T_g of the rubber/metal oxide nanocomposites [27]. The moieties of metal oxide limited the movement of rubber chains by creating crosslinks in the nanocomposites. Consequently, the nanocomposites remain rigid with the increased temperatures.

4. Conclusions

Nanocomposites were synthesized from rubber (ENR-50) and metal oxide (Fe_3O_4). According to the structural analyses, the nanocomposites showed strong interactions between filler (Fe_3O_4) and matrix (ENR-50); this could also be attributed to the possible ring opening reaction of the epoxide units during nanocomposite synthesis. The matrix/filler interactions presented new characteristics of the synthesized nanocomposites, which is also consistent with the morphological analyses that demonstrated different levels of filler adhesions and dispersions in the rubber matrix.

Author Contributions: Conceptualization, O.S.D. and K.A.-Z.; methodology, O.S.D.; software, K.A.-Z.; validation, O.S.D.; formal analysis, O.S.D.; investigation, O.S.D. and K.A.-Z.; resources and data curation, K.A.-Z.; writing—original draft preparation, O.S.D.; writing—review and editing, K.A.-Z.; visualization, K.A.-Z.; supervision, O.S.D.; project administration, O.S.D.; funding acquisition, O.S.D. All authors have read and agreed to the published version of the manuscript.

Funding: This research received no external funding.

Conflicts of Interest: The authors declare no conflicts of interest.

References

1. Hassan, T.; Salam, A.; Khan, A.; Khan, S.U.; Khanzada, H.; Wasim, M.; Khan, M.Q.; Kim, I.S. Functional nanocomposites and their potential applications: A review. *J. Polym. Res.* **2021**, *28*, 36. [CrossRef]
2. Darwish, M.S.; Mostafa, M.H.; Al-Harbi, L.M. Polymeric nanocomposites for environmental and industrial applications. *Int. J. Mol. Sci.* **2022**, *23*, 1023. [CrossRef]

3. Nguyen, M.D.; Tran, H.V.; Xu, S.; Lee, T.R. Fe_3O_4 nanoparticles: Structures, synthesis, magnetic properties, surface functionalization, and emerging applications. *Appl. Sci.* **2021**, *11*, 11301. [CrossRef] [PubMed]
4. Dong, L.; Chen, G.; Liu, G.; Huang, X.; Xu, X.; Li, L.; Zhang, Y.; Wang, J.; Jin, M.; Xu, D.; et al. A review on recent advances in the applications of composite Fe3O4 magnetic nanoparticles in the food industry. *Crit. Rev. Food Sci. Nutr.* **2024**, *64*, 1110–1138. [CrossRef] [PubMed]
5. Niu, Y.; Zhang, X.; Kang, Y.; Sun, P.; Liu, H.; Xiao, Z.; Zhao, D. Magnetic microcapsules based on Fe_3O_4 nanoparticles: Preparation, properties, and applications. *Mater. Today Commun.* **2024**, *39*, 108660. [CrossRef]
6. Nordin, A.H.; Ahmad, Z.; Husna, S.M.N.; Ilyas, R.A.; Azemi, A.K.; Ismail, N.; Nordin, M.L.; Ngadi, N.; Siti, N.H.; Nabgan, W.; et al. The state of the art of natural polymer functionalized Fe3O4 magnetic nanoparticle composites for drug delivery applications: A review. *Gels* **2023**, *9*, 121. [CrossRef]
7. Mallakpour, S.; Tukhani, M.; Hussain, C.M. Sustainable plant and microbes-mediated preparation of Fe_3O_4 nanoparticles and industrial application of its chitosan, starch, cellulose, and dextrin-based nanocomposites as catalysts. *Int. J. Biol. Macromol.* **2021**, *179*, 429–447. [CrossRef] [PubMed]
8. Faustini, M.; Nicole, L.; Ruiz-Hitzky, E.; Sanchez, C. History of organic–inorganic hybrid materials: Prehistory, art, science, and advanced applications. *Adv. Funct. Mater.* **2018**, *28*, 1704158. [CrossRef]
9. Tian, J.; Feng, Y.K.; Xu, Y.S. Synthesis of magnetite nanoparticles with PDLLA corona. *J. Polym. Res.* **2006**, *13*, 343–347. [CrossRef]
10. Durmus, Z.; Kavas, H.; Toprak, M.S.; Baykal, A.; Altınçekiç, T.G.; Aslan, A.; Bozkurt, A.; Coşgun, S. L-lysine coated iron oxide nanoparticles: Synthesis, structural and conductivity characterization. *J. Alloys Compd.* **2009**, *484*, 371–376. [CrossRef]
11. Koneracka, M.; Múčková, M.; Závišová, V.; Tomašovičová, N.; Kopčanský, P.; Timko, M.; Juríková, A.; Csach, K.; Kavečanský, V.; Lancz, G. Encapsulation of anticancer drug and magnetic particles in biodegradable polymernanospheres. *J. Phys. Condens. Matter* **2008**, *20*, 204151. [CrossRef]
12. Arsalani, N.; Fattahi, H.; Nazarpoor, M. Synthesis and characterization of PVP-functionalized superparamagnetic Fe3O4 nanoparticles as an MRI contrast agent. *Express Polym. Lett.* **2010**, *4*, 329–338. [CrossRef]
13. Unal, B.; Toprak, M.S.; Durmus, Z.E.H.R.A.; Sözeri, H.; Baykal, A. Synthesis, structural and conductivity characterization of alginic acid–Fe3O4 nanocomposite. *J. Nanoparticle Res.* **2010**, *12*, 3039–3048. [CrossRef]
14. Reddy, M.J.; Chu, P.P.; Kumar, J.S.; Rao, U.S. Inhibited crystallization and its effect on conductivity in a nano-sized Fe oxide composite PEO solid electrolyte. *J. Power Sources* **2006**, *161*, 535–540. [CrossRef]
15. Montoya, P.; Jaramillo, F.; Calderón, J.; De Torresi, S.C.; Torresi, R.M. Evidence of redox interactions between polypyrrole and Fe_3O_4 in polypyrrole–Fe_3O_4 composite films. *Electrochim. Acta* **2010**, *55*, 6116–6122. [CrossRef]
16. Ashjari, M.; Mahdavian, A.R.; Ebrahimi, N.G.; Mosleh, Y. Efficient dispersion of magnetite nanoparticles in the polyurethane matrix through solution mixing and investigation of the nanocomposite properties. *J. Inorg. Organomet. Polym. Mater.* **2010**, *20*, 213–219. [CrossRef]
17. Ding, X.; Han, D.; Wang, Z.; Xu, X.; Niu, L.; Zhang, Q. Micelle-assisted synthesis of polyaniline/magnetite nanorods by in situ self-assembly process. *J. Colloid Interface Sci.* **2008**, *320*, 341–345. [CrossRef]
18. Ahmad, S.H.; Abdullah, M.H.; Hui, D.; Yusoff, A.N.; Puryanti, D. Magnetic and microwave absorbing properties of magnetite–thermoplastic natural rubber nanocomposites. *J. Magn. Magn. Mater.* **2010**, *322*, 3401–3409. [CrossRef]
19. Mahmood, W.A.K.; Azarian, M.H. Thermal, surface, nanomechanical and electrical properties of epoxidized natural rubber (ENR-50)/polyaniline composite films. *Curr. Appl. Phys.* **2015**, *15*, 599–607. [CrossRef]
20. Hamzah, R.; Bakar, M.A.; Dahham, O.S.; Zulkepli, N.N.; Dahham, S.S. A structural study of epoxidized natural rubber (ENR-50) ring opening under mild acidic condition. *J. Appl. Polym. Sci.* **2016**, *133*, 44123. [CrossRef]
21. Dahham, O.S.; Hamzah, R.; Bakar, M.A.; Zulkepli, N.N.; Dahham, S.S.; Ting, S.S. NMR study of ring opening reaction of epoxidized natural rubber in presence of potassium hydroxide/isopropanol solution. *Polym. Test.* **2017**, *59*, 55–66. [CrossRef]
22. Azman, W.W.M.N.; Jaafar, J.; Salleh, W.N.W.; Ismail, A.F.; Othman, M.H.D.; Rahman, M.A.; Rasdi, F.R.M. Highly selective SPEEK/ENR blended polymer electrolyte membranes for direct methanol fuel cell. *Mater. Today Energy* **2020**, *17*, 100427. [CrossRef]
23. Mahmood, W.A.K.; Khan, M.M.R.; Azarian, M.H. Sol-gel synthesis and morphology, thermal and optical properties of epoxidized natural rubber/zirconia hybrid films. *J. Non-Cryst. Solids* **2013**, *378*, 152–157. [CrossRef]
24. Sengloyluan, K. Silica-Reinforced Natural Rubber: Use of Natural Rubber Grafted with Chemical Functionalities as Compatibilizer. Ph.D. Thesis, University of Twente, Enschede, The Netherlands, 2015.
25. Wei, K.K.; Leng, T.P.; Keat, Y.C.; Osman, H.; Ying, L.B. Enhancing compatibility in epoxy/vulcanized natural rubber (VNR)/Graphene nano-platelets (GNP) system using epoxidized natural rubber (ENR-50). *Compos. Part B Eng.* **2019**, *174*, 107058. [CrossRef]
26. Sharifuddin, S.M.; Mat Nor, M.S.; Pabli, F.A.M.; Luangchuang, P.; Chueangchayaphan, W.; Sulaiman, M.A. Thermal and dynamic mechanical behaviours of CCTO/ENR-25 composite. In *Materials Science Forum*; Trans Tech Publications Ltd.: Baech, Switzerland, 2020; Volume 1010, pp. 274–279.

27. Barrera, G.; Sciancalepore, C.; Messori, M.; Allia, P.; Tiberto, P.; Bondioli, F. Magnetite-epoxy nanocomposites obtained by the reactive suspension method: Microstructural, thermo-mechanical and magnetic properties. *Eur. Polym. J.* **2017**, *94*, 354–365. [CrossRef]
28. Dahham, O.S.; Zulkepli, N.N. Robust interface on ENR-50/TiO_2 nanohybrid material based sol-gel technique: Insights into synthesis, characterization and applications in optical. *Arab. J. Chem.* **2020**, *13*, 6568–6579. [CrossRef]
29. Dahham, O.S.; Hamzah, R.; Noriman, N.Z.; Alakrach, A.M.; Idrus, S.S.; Shayfull, Z.; Adam, T. The influences of zirconium dioxide on ENR-25/ZrO_2 composites: FTIR and TGA Analysis. *J. Phys. Conf. Ser.* **2018**, *1019*, 012055. [CrossRef]
30. Alzamili, K.; Dahham, O.S. Synthesis and characterization of nano hybrid materials from epoxidized natural rubber/zirconium dioxide (ENR-50/ZrO_2). *AIP Conf. Proc.* **2025**, *3169*, 050008.
31. Takai, Z.I.; Mustafa, M.K.; Asman, S.; Sekak, K.A. Preparation and characterization of magnetite (Fe_3O_4) nanoparticles by sol-gel method. *Int. J. Nanoelectron. Mater* **2019**, *12*, 37–46.
32. Bakar, M.A.; Tan, W.L.; Bakar, N.A. A simple synthesis of size-reduce magnetite nano-crystals via aqueous to toluene phase-transfer method. *J. Magn. Magn. Mater.* **2007**, *314*, 1–6. [CrossRef]
33. Wen, X.; Yang, J.; He, B.; Gu, Z. Preparation of monodisperse magnetite nanoparticles under mild conditions. *Curr. Appl. Phys.* **2008**, *8*, 535–541. [CrossRef]
34. Motaung, T.E.; Luyt, A.S.; Thomas, S. Morphology and properties of NR/EPDM rubber blends filled with small amounts of titania nanoparticles. *Polym. Compos.* **2011**, *32*, 1289–1296. [CrossRef]
35. Bautin, V.A.; Rytov, R.A.; Nalench, Y.A.; Chmelyuk, N.S.; Antoshina, I.A.; Usov, N.A. Specific absorption rate in quasispherical and elongated aggregates of magnetite nanoparticles: Experimental characterization and numerical simulation. *Ceram. Int.* **2023**, *49*, 16379–16384. [CrossRef]
36. Bijarimi, M.; Ahmad, S.; Rasid, R. Mechanical, thermal and morphological properties of poly (lactic acid)/epoxidized natural rubber blends. *J. Elastomers Plast.* **2014**, *46*, 338–354. [CrossRef]
37. Kassaee, M.Z.; Motamedi, E.; Majdi, M. Magnetic Fe_3O_4-graphene oxide/polystyrene: Fabrication and characterization of a promising nanocomposite. *Chem. Eng. J.* **2011**, *172*, 540–549. [CrossRef]
38. Dallas, P.; Georgakilas, V.; Niarchos, D.; Komninou, P.; Kehagias, T.; Petridis, D. Synthesis, characterization and thermal properties of polymer/magnetite nanocomposites. *Nanotechnology* **2006**, *17*, 2046. [CrossRef]